

Low hardness indentation mechanics in CN_x coatings

A.S. Bhattacharyya^{1, 2 §}

Department of Metallurgical and Materials Engineering, Central University of Jharkhand,
Ranchi 835205, India¹
Centre of Excellence in Green and Efficient Energy Technology, Central University of Jharkhand,
Ranchi 835205, India²

§Corresponding author:
2006asb@gmail.com, arnab.bhattacharya@cuja.ac.in

ABSTRACT

Carbon-Nitride (CN_x) coatings deposited by means of plasma vapour deposition led to the formation of g-C₃N₄ phase in a mainly amorphous matrix, Nanoindentation was performed on these coatings deposited on 304 SS (stainless steel) substrates. The positioning of the indentation i.e inside the grain formed and at the boundary showed prolific features pertaining to the understanding of extension of plastic volume and variations in interfacial fracture energies and the role played by ductile substrates in preventing damage to a component. The amorphous nature of the grain boundary is detrimental to the overall performance of the system as confirmed by the strain rate variations and has been suggested to get rid of by post deposition treatment

KEYWORDS: CN_x, nanoindentation, low hardness, substrate effect

INTRODUCTION

Carbon Nitride (CN_x) coatings have applications as conductive wear resistant protective coatings for magnetic devices, bioimplants and sensors [1, 2]. They have a band gap of 2.7 eV and are used for photocatalysis [3, 4] Their sensing applications comes from the N-H groups formed [6]. The polymer Triazine (C₃N₃) is the first ever compound out of C and N derivatives In the general chemical structure C₃N₄, the C atoms are in both sp³ and sp² states with the former being tetrahedrally whereas the later as a planar structure bonded to N atoms.

Carbon nitrides can exist in different phases viz., α-C₃N₄, β-C₃N₄, cubic C₃N₄, pseudocubic C₃N₄, and graphite C₃N₄ The β-C₃N₄ phases has been theoretically predicted to have hardness comparable to diamond [6], experimental evidence of which has been found in congruence with other phases in a nanocomposite film giving high hardness. The formation of isolated β-C₃N₄ phase has still not been achieved [7-9]. The CN_x system being deposited in the form of films having various complexion of phases help their use in device fabrication and performance [10-14]. There is however ambiguity and lack of control on the complexion of the phases obtained on being deposited as a thin coating. The nanomechanical characterizations performed have been mostly case-specific and biased towards showing the effectiveness of the techniques and not equally devoted to find the material properties. An attempt here has therefore been made to understand the material (CN_x) properties more based on the indentation involving depth sensing techniques.

MATERIALS & METHODS

CN_x Coatings were deposited on Si (100) and 304 SS substrates by magnetron sputtering using a graphite target and N₂ gas as well as plasma enhanced chemical vapour deposition (PECVD) using N₂/C₂H₂ precursor gases with a Nitrogen gas flow. Both the methods consisted of an initial evacuation to a high vacuum (~10⁻⁵-10⁻⁶ Torr) using diffusion and turbomolecular pumps [15, 16]. XRD was done to detect the crystallinity. The microstructure of the films was obtained by optical microscope (Leica, Germany) Nanoindentation studies were performed by XP (MTS, USA) to determine the mechanical properties.

RESULTS & DISCUSSIONS

The XRD plot of PVD (Sputtered) CN_x showed highly amorphous nature with no prominent peak apart from a broad peak around 30°. The CVD-CN_x films however showed hints of crystallinity as some peaks were detectable and given in Table (inset). The most intense peak at 73 ° was due Si (100) substrate. The growth of mainly **g-C₃N₄** phase took place while deposition [17]. The broad peak indicating amorphous nature was centered around a higher 2θ value of 36° compared to the PVD-CN_x films which occurs due to lower lattice parameters (Fig 1a). Crystallites of larger sizes were formed in CVD-CN_x films as observed in the optical images (Fig 1b, c)

Nanoindentations performed on PVD-CN_x coatings have been reported earlier. The CVD-CN_x films having larger crystallite size showed variations in the P-h plot based on the indenter positioning and consequently the hardness (H) and modulus (E) as also reported previously [18]. Indentations performed inside the grains (A) gave a better mechanical response than at the grain boundaries (B) (Fig 2a, b) Formation of soft **g-C₃N₄** phase as found from XRD provided reduced H and E values compared to conventional protective coatings The hardness was found to increase after **100 nm** inside the grain region indicating strain hardening. The effect was not that prolific at the GBs. An increase of **50 MPa** in hardness due to penetration of **300 nm** can be seen (Fig 2c). The higher plastic deformation was also associated with changed tip-sample contact from Hertzian ($P=kh$) to $P=kh^n$ ($1 \leq n \leq 2$) as the sharper sides of the three sides of the indenter come in contact (shown in the inset). The change in elastic modulus E on the other hand is related to the damage that is occurring during the indentation and is the pre-requisite phenomenon before fracture (Fig 2d). The fracture process manifests itself by means of discontinuity in the loading portions in the form of pop-ins. Although no such evidence was found in the P-h plot, the derivative of the loading portion of the plots showed formation of subsurface micro-cracks for indentations inside the grains. (A) during the steady increase in the rate of indentation loading. The indentation rate was much subtle at the GB (B) and distinct transformation in the tip-sample contact nature can be seen to occur at **200 nm** (Fig 3 a, b, c).

There exists a plastic zone below the indentation region having a radius (r_p) as per eq 1, (σ_y is the yield stress) from where the hardness is determined [19]. This radius is again related to the interfacial fracture energy Γ_i as per eq 2 [20]. The parameters for four indentation depth determined for test A are given in Table 1 The r_p and Γ_i showed a steady increase with depth. New dislocations are created in front of crack tip in a zone defined by r_p and therefore an increase in r_p with depth of penetration suggest higher number of dislocations causing strain hardening

$$r_p = \sqrt{\frac{3P}{2\pi\sigma_y}}; \sigma_y = 2.8 H \quad (1)$$

$$r_p = \frac{1}{\pi} \left(\frac{\Gamma_i}{H} \right) \quad (2)$$

Table 1: Parameters and calculate plastic zone radius (r_p) and interfacial fracture energies for nanoindentation carried inside the grain (A) and at the grain boundary (B)

Depth h (nm)	A(Grain)				B (Grain boundary)			
	Load P (mN)	Hardness H (GPa)	r_p (μm)	Γ_i (J/m ²)	Load P (mN)	Hardness H (GPa)	r_p (μm)	Γ_i (J/m ²)
100	0.05	0.075	0.33	78	0.01	0.037	0.21	24
200	0.15	0.08	0.56	140	0.075	0.04	0.56	70
300	0.35	0.11	0.73	252	0.12	0.049	0.64	98
400	0.65	0.125	0.93	365	0.22	0.049	0.87	134

For indentations performed at the GBs, the r_p did not show a steady increase. There were instances where it seemed to attain saturation (300 nm) but increased thereafter. For films deposited on softer substrate, the effect of substrate starts at about 1/10th of the coating thickness causing the H and E values to start decreasing with higher depths of penetration. For cases where the coatings are of lower hardness than the substrate material, (as in this case) the effect of substrate can gets manifested in more than one way. The reinitiation of the increase in r_p is one of them where it is now no longer confined to the coating region but gets extends to the 304SS substrate (as shown in the inset- Fig 3d). This causes the strain

hardening to start in the substrate itself where the coating has no role to play. The only effect it might have on the coating is its plastic flow surrounding the indent. In case of harder and brittle substrate, which will be able to accommodate the elastic strain gradient leading to strain hardening, radial and lateral cracks may appear as reported earlier. The interfacial fracture energy plot shows how the interface gets toughened as the dislocations pile up at the interface in case of grain centre testing. For grain boundary indents, the extent of plastic deformation is less as there is no specific crystallographic pattern developed. The region mainly consists of mixed hybridised (sp , sp^2 and sp^3) phases of carbon and are prone to brittle failure following damage as also depicted from the decrease of Γ_i (Fig 3e).

The change in elastic modulus is associated with damage which can be visualized by a damage index D being the derivative dE/dh as shown in Fig 3f. The D_B index associated with grain boundary indentation, The stainless-steel substrate accommodates the accumulated strains and plays a beneficial role in decreasing the developed damage index avoiding brittle failure. The strain rates which quantify the rate of deformations were also plotted for the two cases with respect to load and depth (Fig 4) and quite expectedly were higher for the GB indentations. The 304SS substrate was found absorbing the strain gradient in both the cases from depth of penetration of 220 nm at a considerable distance from the interface.

The $g-C_3N_4$ phase has use in photocatalysis. It has also been applied over steel components for corrosion protection. The inclusive amorphous carbon phase present having mixed hybridization therefore needs to be transformed into hard phases of carbon which requires nitriding and heat treatment post deposition. Another alternative approach can be using a tetramethyl silane i.e. $Si(CH_3)_4$ precursor which nullifies the possibility of carbonaceous amorphous phases but keeps the possibility of $g-C_3N_4$ alive [21].

CONCLUSIONS

A comparative investigation of carbon nitride films deposited by PVD (magnetron sputtering) and CVD (PECVD) techniques was performed. The PVD-CNx were found amorphous while crystallinity persisted in CVD-CNx giving larger sized grains. Nanoindentation performed on CVD-CNx films showed variations based on positioning of the indenter. Indentations performed on the grains caused strain hardening and increased interfacial fracture energy. For indentations on the grain boundaries, the substrate was found to absorb the accumulated strain developed due to indentation and was instrumental in lowering down the damage. Strain rates showed higher variations for indentations made at the grain boundaries. A post deposition heat treatment, nitriding and usage of a different precursor is suggested to avoid the grain boundary affecting the overall mechanical strength of the system.

ACKNOWLEDGEMENTS

The author hereby thanks Dr. S. K. Mishra for experimental studies.

DECLARATIONS

Compliance with Ethical Standards

The manuscript has not been submitted in parallel either in full or partially to any other journal.

Conflict of interest

There is no conflict of interest among the authors.

Research Data Policy and Data Availability Statements

Data shall be provided on request.

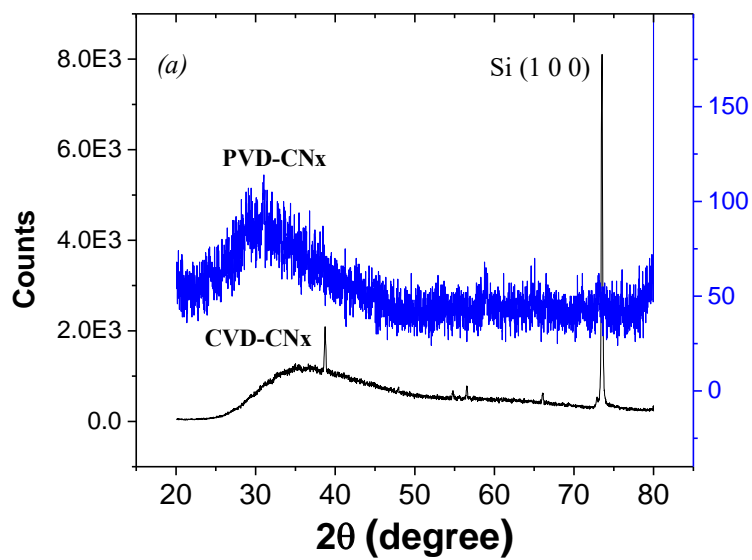
FUNDING

No funding was received for conducting the research.

REFERENCE

1. Rashid M et al Manufacturing and Characterization of a Carbon-Based Amorphous (a-CNx) Coating Material Nanomanufacturing and Metrology (2018) 1:156–170 [https://doi.org/10.1007/s41871-018-0014-y\(0123456789\(\).,-volV\)\(0123](https://doi.org/10.1007/s41871-018-0014-y(0123456789().,-volV)(0123)

2. Idris AO, Oseghe EO, Msagati TAM, Kuvarega AT, Feleni U, Mamba B. Graphitic Carbon Nitride: A Highly Electroactive Nanomaterial for Environmental and Clinical Sensing. *Sensors*. 2020; 20(20):5743. <https://doi.org/10.3390/s20205743>
3. Vinodh, R.; Atchudan, R.; Yi, M.; Kim, H.-J. Synthesis and Properties of Carbon Nitride Materials. In *Nanostructured Carbon Nitrides for Sustainable Energy and Environmental Applications*; Elsevier, 2022; pp 1–18.
4. Zhu, J.; Xiao, P.; Li, H.; Carabineiro, S. A. C. Graphitic Carbon Nitride: Synthesis, Properties, and Applications in Catalysis. *ACS Appl. Mater. Interfaces* **2014**, 6 (19), 16449–16465. <https://doi.org/10.1021/am502925j>.
5. Xavier, M. M.; Mathew, S. G-C₃N₄-Based Sensors. In *Synthesis, Characterization, and Applications of Graphitic Carbon Nitride*; Elsevier, 2023; pp 225–248
6. Anjumol, K. S.; Joy, J.; Mathew, S. S.; Maria, H. J.; Spatenka, P.; Thomas, S. Graphitic Carbon Nitride-Based Nanocomposites. In *Synthesis, Characterization, and Applications of Graphitic Carbon Nitride*; Elsevier, 2023; pp 59–76.
7. Bhattacharyya, A. S.; Mishra, S. K. Raman Studies on Nanocomposite Silicon Carbonitride Thin Film Deposited by r.f. Magnetron Sputtering at Different Substrate Temperatures. *J. Raman Spectrosc.* **2010**, 41 (10), 1234–1239. <https://doi.org/10.1002/jrs.2588>.
8. A. S Bhattacharyya, S.K Mishra, S. Mukherjee, Journal of Vacuum Science and Technology A 28 (2010) 505-509.
9. S. K. Mishra, A. S. Bhattacharyya, P. K. P. Rupa, L.C. Pathak Nanoscience and Nanotechnology Letters, 4 (2012) 1-6.
10. Jia, C.; Yang, L.; Zhang, Y.; Zhang, X.; Xiao, K.; Xu, J.; Liu, J. Graphitic Carbon Nitride Films: Emerging Paradigm for Versatile Applications. *ACS Appl. Mater. Interfaces* **2020**, 12 (48), 53571–53591. <https://doi.org/10.1021/acsami.0c15159>.
11. Chang Liu, Stephanie Busse, Jian Liu, Robert Godin. Aminosilanized Interface Promotes Electrochemically Stable Carbon Nitride Films with Fewer Trap States on FTO for (Photo)electrochemical Systems. *ACS Applied Materials & Interfaces* **2023**, Article ASAP.
12. Zichen Xu, Yongzhi Yu, Jian Zhao, Zhixin Liao, Yanyan Sun, Si Cheng, Shaohua Gou. A Unique Chemo-photodynamic Antitumor Approach to Suppress Hypoxia via Ultrathin Graphitic Carbon Nitride Nanosheets Supported a Platinum(IV) Prodrug. *Inorganic Chemistry* **2022**, 61 (50), 20346-20357. <https://doi.org/10.1021/acs.inorgchem.2c02806>
13. Zhou Chen, Yihong Lan, Yubin Hong, Weiguang Lan. Review of 2D Graphitic Carbon Nitride-Based Membranes: Principles, Syntheses, and Applications. *ACS Applied Nano Materials* **2022**, 5 (9), 12343-12365. <https://doi.org/10.1021/acsanm.2c03416>
14. Paolo Giusto, Baris Kumru, Daniel Cruz, Markus Antonietti. Optical Anisotropy of Carbon Nitride Thin Films and Photografted Polystyrene Brushes. *Advanced Optical Materials* **2022**, 10 (4) <https://doi.org/10.1002/adom.202101965>
15. Mishra, S. K.; Mahanta, P.; Sen, S.; Pathak, L. C. Effect of Nitrogen on the Growth of Carbon Nitride Thin Films Deposited by RF Plasma Enhanced Chemical Vapor Deposition. *Nanosci. Nanotechnol. Lett.* **2012**, 4 (1), 90–94. <https://doi.org/10.1166/nnl.2012.1285>.
16. A S Bhattacharyya, P Mohanta. Clustering in hydrogenated carbon nitride films: surface proliferation of nitrogen induced carbonaceous growth. *Authorea*.2023
17. P. Fageria et al RSC Adv., 2015,5, 80397-80409 <https://doi.org/10.1039/C5RA12463H>
18. Z. D. Sha, Q. Wan, Q. X. Pei, S. S. Quek, Z. S. Liu, Y. W. Zhang & V. B. Shenoy, Scientific Reports, 4 : 7437 (2014)
19. Zak, S., Trost, C.O.W., Kreiml, P. *et al.* Accurate measurement of thin film mechanical properties using nanoindentation. *Journal of Materials Research* **37**, 1373–1389 (2022). <https://doi.org/10.1557/s43578-022-00541-1>
20. R. Dash, Kushal Bhattacharyya, A.S. Bhattacharyya, Synergistic fractural features observed in Ti-B-Si-C hard coatings on enhancing the sharpness of nano indenters, International Journal of Refractory Metals and Hard Materials,116, 2023, 106373, <https://doi.org/10.1016/j.ijrmhm.2023.106373>.
21. Plujat, B, Glénat, H, Bousquet, A, et al. SiCN:H thin films deposited by MW-PECVD with liquid organosilicon precursor: Gas ratio influence versus properties of the deposits. *Plasma Process Polym.* 2020; 17:1900138. <https://doi.org/10.1002/ppap.201900138>



S. No	2θ (deg)	Counts	d space (Å)	Relative Intensity	Phase
1	38.72	2093	2.698	26	g-C ₃ N ₄ (101)
2	54.86	591	1.942	7	-
3	56.58	766	1.887	9	g-C ₃ N ₄ (110)
4	66.06	627	1.641	8	-
5	73.50	8104	1.495	100	Si (100)

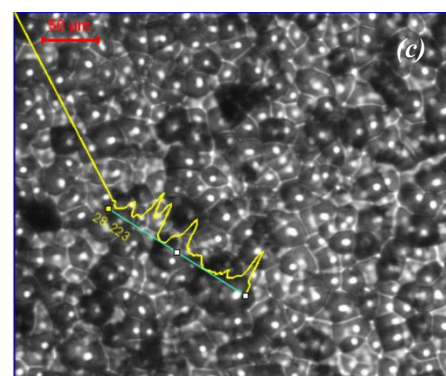
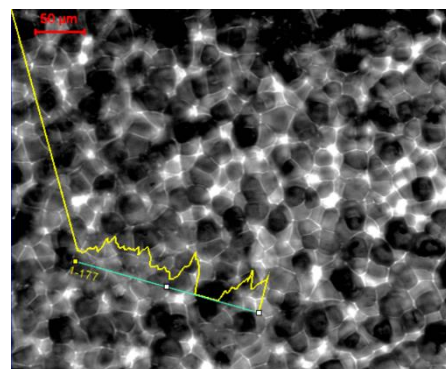


Fig 1 (a) XRD and optical images of (b) CVD-CNx and (c) PVD-CNx coatings

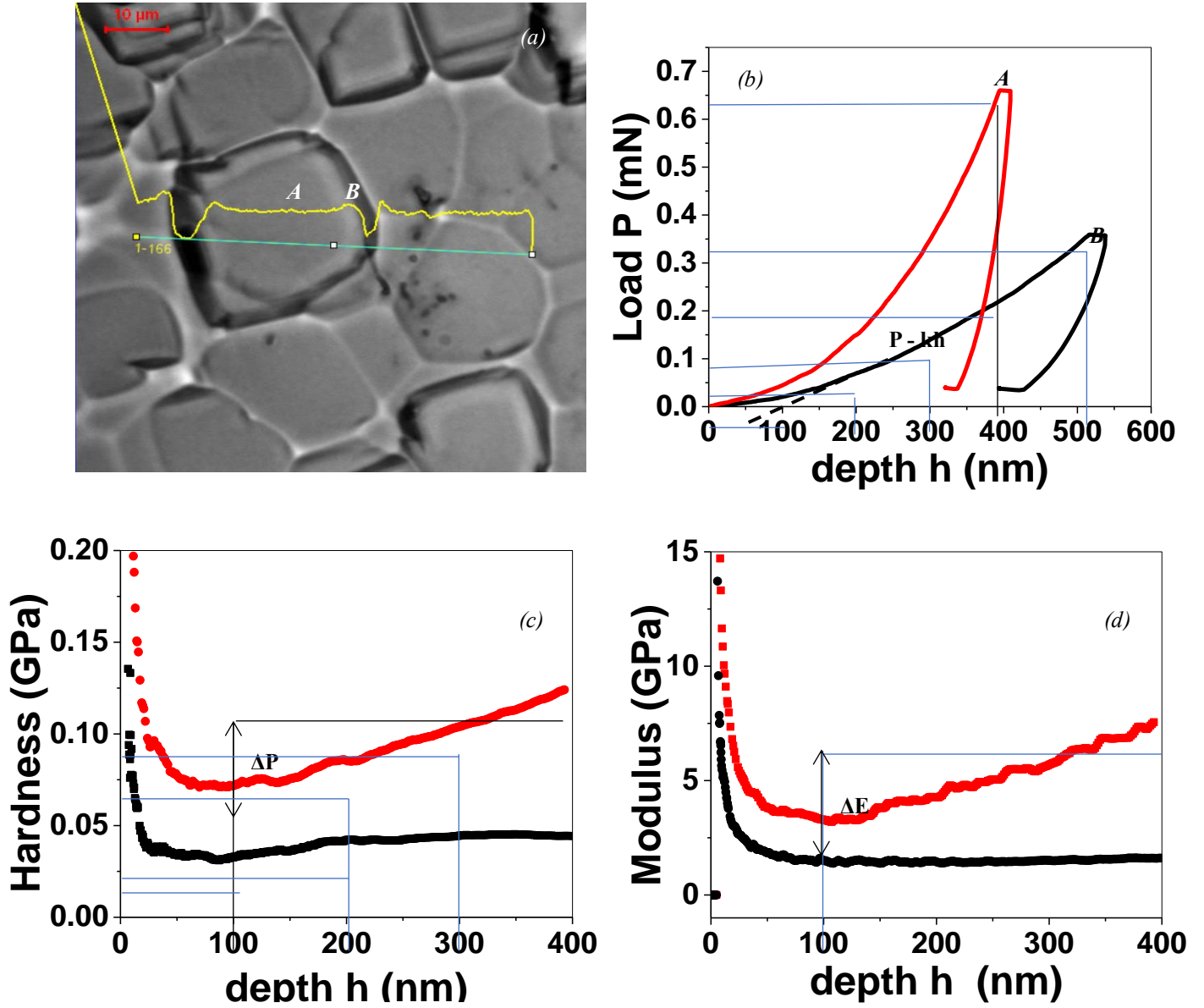


Fig 2 (a) Optical images of CVD-CN_x and Nanoindentation (b) P-h plots at different regions of the microstructure with corresponding (c) Hardness and (d) Modulus variations

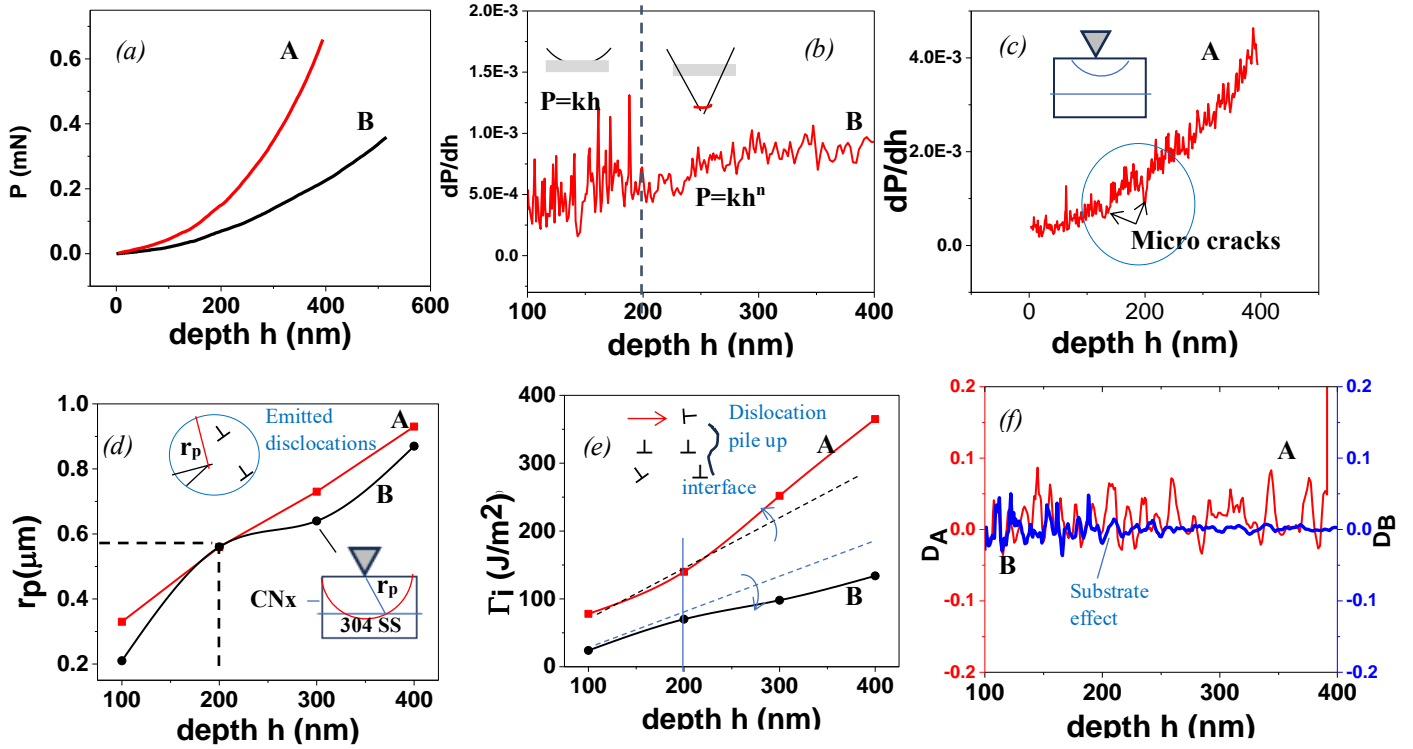


Fig 3 (a) Loading portions of the nanoindent P - h plots. Differential hardness for (b) grain boundary and (c) grain regions (d) variation of plastic depth and (e) interfacial fracture energies with depth of penetration and (f) the variation of damage index with depth for penetration inside grain and at the grain boundaries.

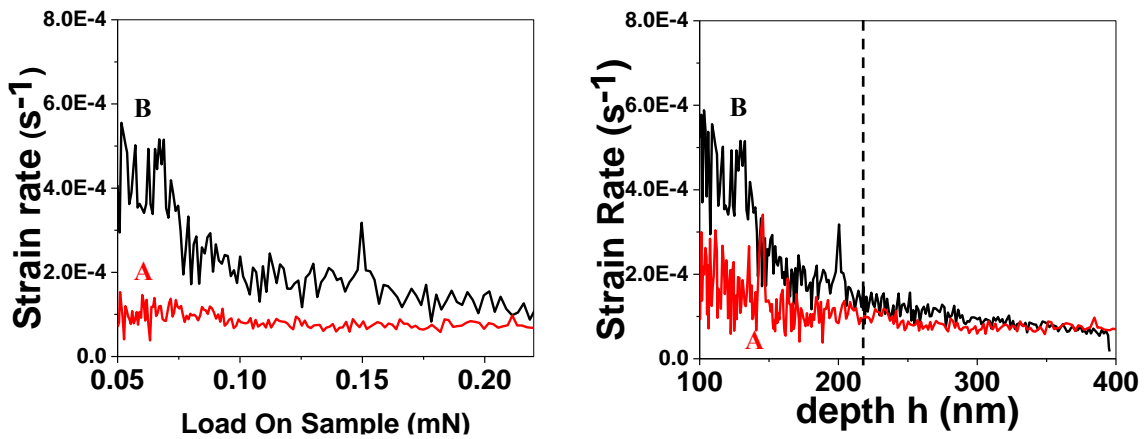


Fig 4. Strain rate variations with respect to (a) load applied and (b) depth of penetration

